IEEE Access
Multidisciplinary | Rapid Review | Open Access Journal

Date of publication xxxx 00, 0000, date of current version xxxx 00, 0000.

Digital Object Identifier 10.1109/ACCESS.2017.Doi Number

Modified Phase-Shift Scheme for Optimal Transient Response of Dual-Active-Bridge DC/DC Converters Considering the Resistive Impact

Jian Yin[1], (Member, IEEE), Jian Lu[1], Hui Jiang[2], Yitao Liu[1], (Senior Member, IEEE), and Jianchun Peng[1], (Senior Member, IEEE)

[1]College of Mechatronics and Control Engineering, Shenzhen University, Nanshan District, Shenzhen 518060, Guangdong, China;
[2]College of Physics and Optoelectronic Engineering, Shenzhen University, Nanshan District, Shenzhen 518060, Guangdong, China;

Corresponding authors: Jian Yin (jyin@szu.edu.cn) and Hui Jiang (huijiang@szu.edu.cn)

This work was supported in part by the Shenzhen Science and Technology Research Foundation under Grant JCYJ20200109105204077, Grant JCYJ20180305125407996, Grant GJHZ20180928160212241, and Grant JCYJ20190808165201648, and in part by the Shenzhen University Starting Research Program.

ABSTRACT The scattered resistive elements residing in a dual-active-bridge (DAB) dc/dc converter can adversely affect its transient performance especially when the load change is large. Conventional phase-shift methods do not take the resistive impact into account in their modeling and analysis. In this paper, a comprehensive analysis of the detrimental influence on the transient performance of a DAB converter due to resistive elements is presented, based on which a modified phase-shift scheme is proposed to further optimize the transient response of the converter. A DAB prototype is designed to verify the resistive impact discussed and validate the proposed phase-shift scheme. The experimental results confirm that better transient response can be effectively achieved with the proposal.

INDEX TERMS Current bias, dual-active-bridge (DAB), hard switching, phase-shift, single-phase-shift (SPS), transient response.

I. INTRODUCTION

The class of dc/dc converters based on the dual-active-bridge (DAB) topology has become more and more popular in applications where galvanic isolation, bidirectional power conversion, soft switching, and high power density are required [1], such as automotive [2], photovoltaic (PV) [3], [4], dc distribution [5]–[7], and energy storage systems [8], [9]. Fig. 1 depicts a typical diagram of a DAB dc/dc converter, where a high-frequency transformer with the turns ratio of $1:N$ is connected between two full-bridges. The ac voltages of the primary and secondary bridges are v_1 and v_2. The ac currents flowing through the primary and secondary sides of the transformer are i_1 and i_2. V_1 and V_2 are the dc voltages of the primary and secondary dc buses. An auxiliary inductor L is connected in series to either side of the transformer to adjust the power rating of the converter. By properly controlling the waveforms and phases of v_1 and v_2, the DAB converter can be operated at expected modes and function steadily. Several phase-shift

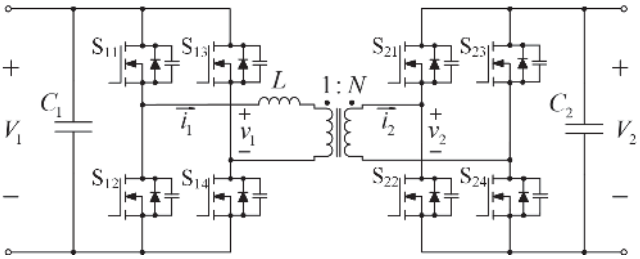

FIGURE 1. DAB dc/dc converter.

modulation and control strategies have been presented to well regulate the output of the converter, [10], such as single-phase-shift (SPS), extended-phase-shift (EPS), dual-phase-shift (DPS), triple-phase-shift (TPS), etc. Fig. 2 shows the typical steady-state waveforms with SPS which is regarded as the simplest method to implement. The output power of the converter can be controlled by adjusting the phase difference in the time domain between

This article has been accepted for publication in a future issue of this journal, but has not been fully edited. Content may change prior to final publication. Citation information: DOI 10.1109/ACCESS.2021.3088839, IEEE Access

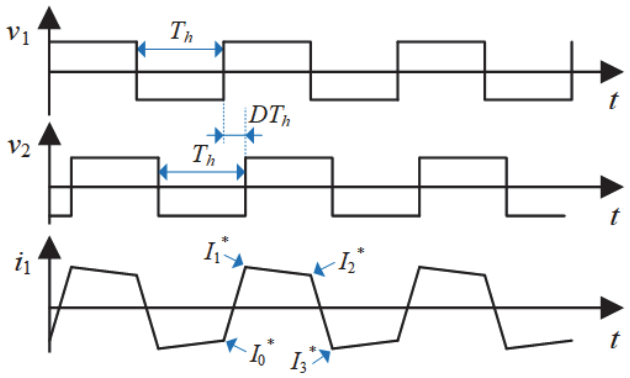

FIGURE 2. Typical steady-state waveforms of v_1, v_2, and i_1 with SPS.

v_1 and v_2, i.e., DT_h, where T_h is one half of the switching cycle and D is the phase-shift ratio ranging from 0 to 0.5.

Although there are diverse control strategies leading to similar steady-state performance of DAB converters, distinct phase-shift schemes implemented can result in essentially different transient performance when the load is changed from one level to another. Optimal transient response, such like shorter settling time, less overshoot and oscillation, is desired. However, if the phase-shift is not suitably optimized, a dc current bias in the high-frequency link may be induced during the transient which can adversely affect the dynamics of the DAB converter [11]–[20]. Li *et al.* discuss the transient performance when different phase-shift schemes are adopted in a DAB converter and propose an asymmetric double-side modulation based on SPS to eliminate the transient dc bias and achieve fast transient response [11]. Subsequently, other transient phase-shift schemes based on SPS with different feedforward algorithms are proposed which can remove the transient dc current bias and avoid magnetic saturation [12]–[14]. In addition, phase-shift schemes based on EPS [15], DPS [16], TPS [17]–[19], and phase-shift with additional zero level [20] are presented to further optimize the dynamic behavior of the converter at the cost of more complicated algorithms. All the aforementioned schemes are based on a simplified model which neglects the effect of the resistive elements in the circuit [21], [22], and therefore cannot give a precise description of the transient performance of the converter especially when the load change is large. In practice, the conventional methods still have deficiency in effectively eliminating the transient dc bias when the power is changed from light load to full load, or reversely.

To better delineate the transient behavior of the DAB dc/dc converter, some more accurate DAB models considering the impact of resistive elements are presented [23]–[25]. However, all these studies focus on the accuracy of prediction of power losses, steady-state behaviors, and dynamic responses, but none of them further discusses the transient performance associated with different phase-shift schemes that are adopted for fast load changing. A three-step phase-shift scheme for three-phase DAB converters is presented in [26], which takes the resistive impact into account and can achieve fast step response without

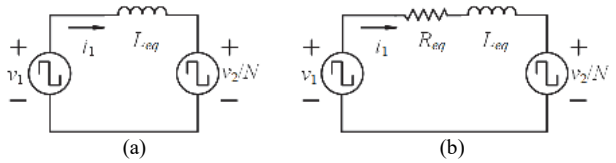

FIGURE 3. Equivalent DAB Models. (a) Neglecting the resistive impact. (b) Considering the resistive impact.

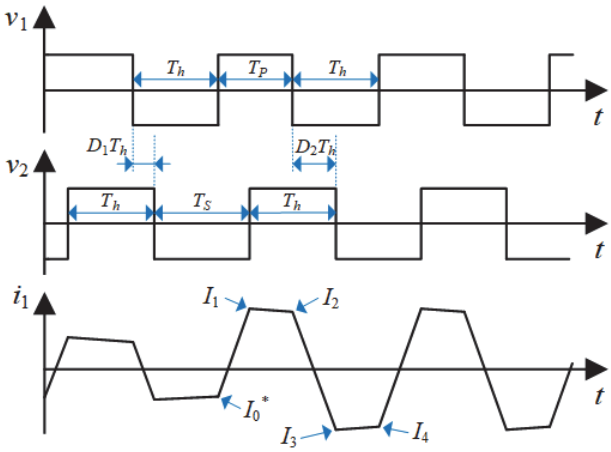

FIGURE 4. Exemplary transient waveforms of v_1, v_2, and i_1 with the phase-shift ratio change from D_1 to D_2 ($D_1 < D_2$).

oscillation. Nevertheless, its analysis on how the resistive elements affect the dynamic response is insufficient, and neither can it be transplanted into a general single-phase DAB converter.

Since conventional phase-shift schemes do not include the resistive impact in their modeling and analysis, they cannot effectively remove the transient dc bias and there will be certain amount of dc bias remaining during the transient, especially when the load change is large. In this paper, a novel phase-shift scheme for single-phase DAB dc/dc converters is proposed to better optimize the transient performance, which is based on a modified circuit model considering the resistive impact. The transient dc current bias can be effectively eliminated, and the converter can reach the steady state within one switching cycle under an abrupt load change. Therefore, optimal transient response is achieved. Comprehensive analysis on the weighting of the resistive impact under different load changes is elaborated to give some design criteria for practical applications. Experimental results are provided to validate the proposed method.

II. TRANSIENT DC CURRENT BIAS WITH NEGLECTION OF THE RESISTIVE IMPACT

A. CONVENTIONAL PHASE-SHIFT SCHEME FOR OPTIMAL TRANSIENT RESPONSE NEGLECTING THE RESISTIVE IMPACT

In order to eliminate the transient current offset in i_1 when the phase difference between v_1 and v_2 is changed, an optimal phase-shift scheme is presented in [11], which is

This article has been accepted for publication in a future issue of this journal, but has not been fully edited. Content may change prior to final publication. Citation information: DOI 10.1109/ACCESS.2021.3088839, IEEE Access

developed based on a simplified DAB model that neglects the resistive elements in the circuit as shown in Fig. 3(a), where v_1 is a square-wave voltage source with the amplitude $\pm V_1$, v_2/N is a square-wave voltage source with the amplitude $\pm V_2/N$, and L_{eq} stands for the equivalent inductance taking the auxiliary and leakage inductances into account. From this model, the steady-state peak currents, i.e., I_0^* to I_3^* in Fig. 2, can be derived in (A1) in Appendix. Furtherly, the optimal phase shifting can be obtained by properly adjusting the pulsewidths of v_1 and v_2 simultaneously, i.e., the positive piece of v_1, T_P, and the negative piece of v_2, T_S. The updated T_P and T_S can be expressed as

$$\begin{cases} T_P = T_h - \dfrac{M}{M+1}(D_2 - D_1)T_h \\ T_S = T_h + \dfrac{1}{M+1}(D_2 - D_1)T_h \end{cases} \tag{1}$$

where D_1 and D_2 are the initial and final phase-shift ratios of the converter, both ranging from 0 to 0.5, and M is the voltage transfer ratio of the converter defined as V_2/NV_1. The exemplary waveforms with this phase-shift scheme are illustrated in Fig. 4, where I_0^* is the peak current in the initial steady-state after which it enters the transient, and I_1 to I_4 are the following transient peak currents. With the optimal phase shifting in (1), I_1 to I_4 will reach their steady-state values in (A1) as expected, and the transient dc bias in i_1 can be theoretically removed. It should be noted that I_4 in Fig. 4 has the same value as I_0^* in Fig. 2 due to the periodicity of the steady-state waveform of i_1.

The above analysis assumes that the total resistance along the circuit loop should be zero. However, there are many resistive elements in a practical DAB converter, such as the winding resistances of the transformer and the auxiliary inductor, and the on-resistances of the switching devices. Therefore, the phase-shift solutions in (1) are not sufficient enough to effectively remove the transient dc bias in i_1 especially when the load change is large. To better estimate the behavior of the converter, a more accurate model considering the effect of the resistive elements should be adopted. In Fig. 3(b), an equivalent resistor R_{eq} is added to model the resistive effect, which stands for the total resistance along the circuit loop. In combination with L_{eq}, the time constant τ of the equivalent circuit model in Fig. 3(b) can be expressed as

$$\tau = \frac{L_{eq}}{R_{eq}} \tag{2}$$

which plays an important role in the following analysis. From this new model, the steady-state peak currents, i.e., I_0^* to I_3^* in Fig. 2, can be re-derived in (A2) in Appendix, which are more accurate compared with the expressions in (A1) and provide a better description of the dynamic behavior of the DAB converter. Correspondingly, the transient peak currents in Fig. 4, i.e., I_1 to I_4, with the conventional phase-shift scheme in (1) can be found as,

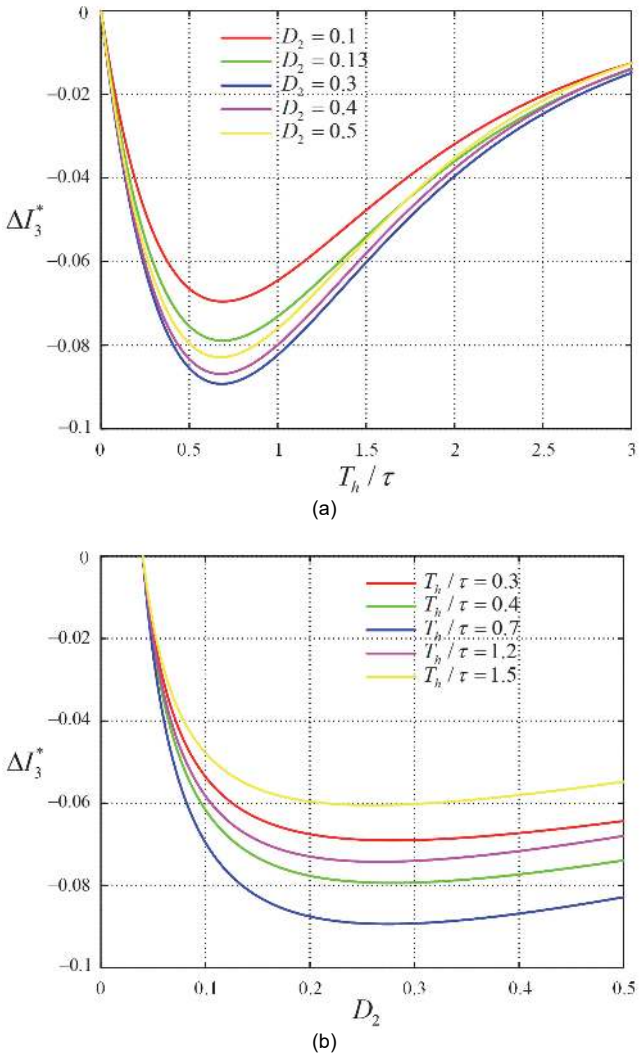

FIGURE 5. Relative current deviation of I_3 under power increase from light load (D_1=0.04). (a) Variation of ΔI_3^* with respect to T_h/τ under different D_2. (b) Variation of ΔI_3^* with respect to D_2 under different T_h/τ.

$$\begin{cases} I_1 = \left[I_0^* - \dfrac{(M+1)V_1}{R_{eq}}\right] e^{-\frac{MD_1 + D_2 T_h}{M+1}\frac{1}{\tau}} + \dfrac{(M+1)V_1}{R_{eq}} \\ I_2 = \left[I_1 + \dfrac{(M-1)V_1}{R_{eq}}\right] e^{-(1-D_2)\frac{T_h}{\tau}} - \dfrac{(M-1)V_1}{R_{eq}} \\ I_3 = \left[I_2 + \dfrac{(M+1)V_1}{R_{eq}}\right] e^{-D_2\frac{T_h}{\tau}} - \dfrac{(M+1)V_1}{R_{eq}} \\ I_4 = \left[I_3 - \dfrac{(M-1)V_1}{R_{eq}}\right] e^{-(1-D_2)\frac{T_h}{\tau}} + \dfrac{(M-1)V_1}{R_{eq}} \end{cases} \tag{3}$$

where I_0^* is given in (A2). By comparing (3) and (A2), it can be found that the transient peak currents deviate from their steady-state values, and the corresponding deviation for each peak current can be expressed as,

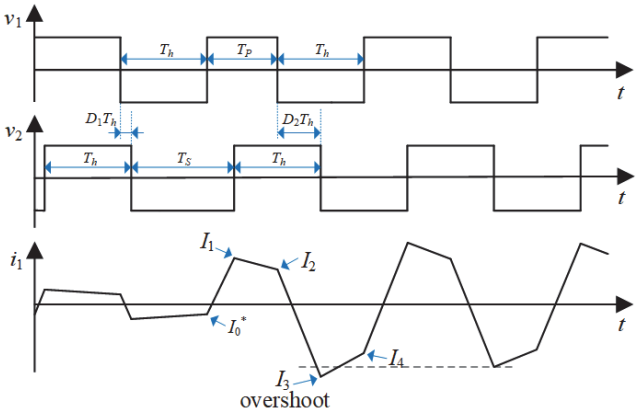

FIGURE 6. Typical transient waveforms of v_1, v_2, and i_1 when the power is increased from light load to full load.

$$\begin{cases} \Delta I_1 = I_1 - I_1^* = \dfrac{2V_1[Me^{-\frac{T_h}{\tau}}\left(1-e^{-\frac{D_2-D_1T_h}{M+1\ \tau}}\right)+e^{-D_2\frac{T_h}{\tau}}\left(1-e^{-M\frac{D_1-D_2T_h}{M+1\ \tau}}\right)]}{R_{eq}(1+e^{-\frac{T_h}{\tau}})} \\ \Delta I_2 = I_2 - I_2^* = \Delta I_1 e^{-(1-D_2)\frac{T_h}{\tau}} \\ \Delta I_3 = I_3 - I_3^* = \Delta I_1 e^{-\frac{T_h}{\tau}} \\ \Delta I_4 = I_4 - I_4^* = \Delta I_1 e^{-(2-D_2)\frac{T_h}{\tau}} \end{cases} \quad (4)$$

The greatest current deviation can be regarded as occurring at I_1 which is the first peak current during the transient, and then it decays exponentially with the time constant τ. Since the DAB converter has the full-range soft switching when $M = 1$ under SPS [27], in the following analysis only the case in voltage matching mode is studied. Among all the transient peak currents, I_3 has the most significant impact on the transient performance of the converter. The relative deviation of I_3 when $M = 1$ can be expressed as

$$\Delta I_3^* = \frac{\Delta I_3}{I_3^*} = e^{-\frac{T_h}{\tau}} \frac{e^{-\frac{T_h}{\tau}}\left(1-e^{-\frac{D_2-D_1T_h}{2\ \tau}}\right)+e^{-D_2\frac{T_h}{\tau}}(1-e^{-\frac{D_1-D_2T_h}{2\ \tau}})}{1-e^{-D_2\frac{T_h}{\tau}}} \quad (5)$$

It can be observed that R_{eq} together with L_{eq} has a joint influence on the transient current deviation in terms of τ instead of an independent resistive impact. What is more, the time-constant related parameter T_h/τ plays an important role in ΔI_3^* from (5), along with the phase-shift ratio change $D_2 - D_1$ and the final phase-shift ratio D_2. Therefore, T_h/τ can be regarded as an independent variable to study the transient current bias. In the next subsections, two cases, load increasing and load decreasing, are examined to reveal how the resistive elements affect the transient performance of the converter.

B. CURRENT BIAS WHEN INCREASING THE POWER FROM LIGHT LOAD (D_1=0.04, D_2>D_1)

When the power of the DAB converter is increased from light load with the initial phase-shift ratio D_1=0.04, the variation of ΔI_3^* with respect to T_h/τ under different final phase-shift ratios D_2 are depicted in Fig. 5(a). In this case, the transient current bias is negative. As T_h/τ increases from zero, for each value of the final phase-shift ratio D_2 the absolute value of ΔI_3^* goes up quickly first and reaches the

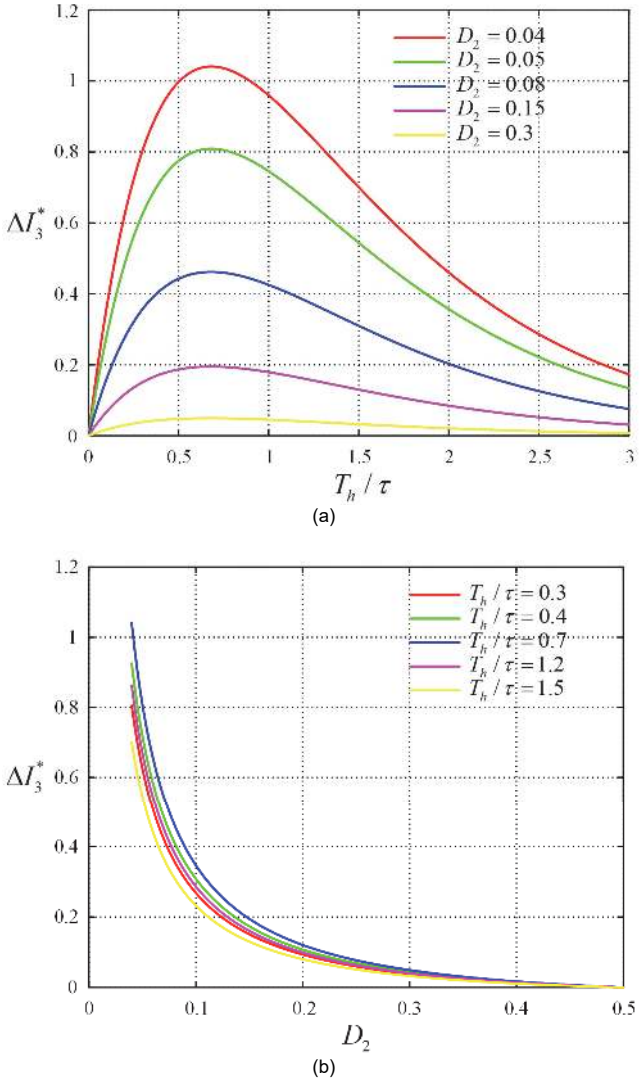

FIGURE 7. Relative current deviation of I_3 under power decrease from full load (D_1=0.5). (a) Variation of ΔI_3^* with respect to T_h/τ with different D_2. (b) Variation of ΔI_3^* with respect to D_2 with different T_h/τ.

peak when T_h/τ is around 0.7. Then, it drops down slowly and approaches to zero again as T_h/τ goes to infinity. When T_h/τ is greater than 3, the absolute value of the relative current deviation is less than 2%, which means that the resistive impact can be neglected. However, when T_h/τ is within the range from 0.3 to 1.5, the absolute value of ΔI_3^* is remarkably large, above 5%, depending on the final load level. If T_h/τ is around 0.7, the resistive elements will have the strongest impact on the transient performance of the converter.

Fig. 5(b) describes the variation of ΔI_3^* with respect to the final phase-shift ratio D_2 for different values of T_h/τ from 0.3 to 1.5. It can be found that the absolute value of ΔI_3^* rises quickly as D_2 starts to increase from 0.04, and it comes down slightly when D_2 passes 0.28. When D_2=0.5, ΔI_3^* can be above 8% of the steady-state peak current depending on T_h/τ. Fig. 6 shows the typical transient waveforms of v_1, v_2, and i_1 when the power is increased

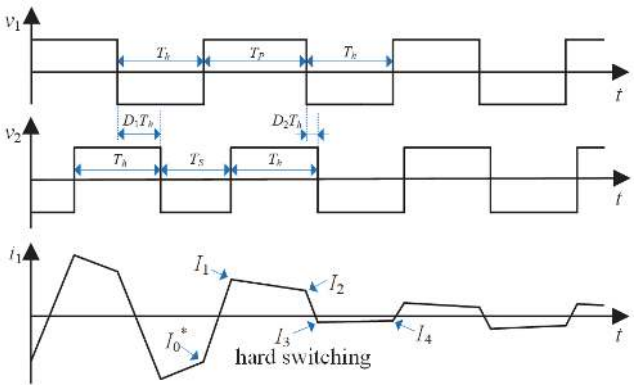

FIGURE 8. Typical transient waveforms of v_1, v_2, and i_1 when the power is decreased from full load to light load.

from light load to full load. Since the transient dc bias is negative, it will reduce the absolute values of all the positive current peaks and increase the absolute values of all the negative current peaks. So I_3 has the most significant impact on the transient performance of the DAB converter where a current overshoot over 8% occurs at worst. The current overshoot flows through the switching devices, the auxiliary inductor, and the high-frequency transformer, and therefore may cause increased current stress and magnetic saturation.

C. CURRENT BIAS WHEN DECREASING THE POWER FROM FULL LOAD (D_1=0.5, D_2<D_1)

When the power of the DAB converter is reduced from full load with the initial phase-shift ratio D_1=0.5, the variation of ΔI_3^* with respect to T_h/τ under different final phase-shift ratios D_2 are depicted in Fig. 7(a). In this case, the transient current bias is positive. As T_h/τ increases from zero, ΔI_3^* goes up quickly at first and reaches the peak when T_h/τ is around 0.7. Then, it drops down slowly and approaches to zero again as T_h/τ goes to infinity. When T_h/τ is greater than 3, the absolute value of the relative current deviation is less than 20%. Since the values of the steady-state peak currents at light load are small, the absolute current deviation is small as well. Therefore, the resistive impact can be regarded as negligible when T_h/τ>3. However, when T_h/τ is within the range from 0.3 to 1.5, ΔI_3^* becomes remarkably large depending on the final load level. If T_h/τ is around 0.7, the resistive elements will have the strongest impact on the transient performance of the converter. The conclusions here are consistent with what are drawn from Fig. 5(a) in subsection B of section II.

Fig. 7(b) describes the variation of ΔI_3^* with respect to the final phase-shift ratio D_2 for different values of T_h/τ from 0.3 to 1.5. It can be found that ΔI_3^* rises slowly as D_2 starts to decrease from 0.5, and it grows faster and faster when D_2 gets close to 0.04. When D_2=0.04, ΔI_3^* can be above 80% or even over 100% of the steady-state peak value depending on T_h/τ. Fig. 8 shows the typical transient waveforms of v_1, v_2, and i_1 when the power is decreased from full load to light

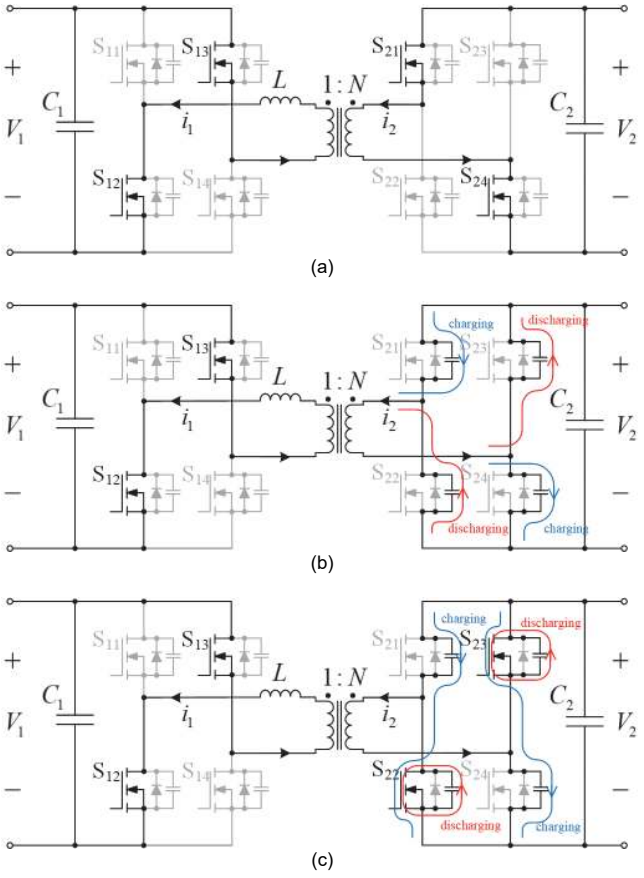

FIGURE 9. Current flowing loops before and after I_3 when I_3 is close to zero. (a) S_{21} and S_{24} on, S_{22} and S_{23} off, before I_3. (b) S_{21} to S_{24} off, during dead-time. (c) S_{22} and S_{23} on, S_{21} and S_{24} off, after dead-time.

load. Since the transient dc bias is positive, it will increase the absolute values of all the positive current peaks and reduce the absolute values of all the negative current peaks. So I_3 has the most significant impact on the transient performance of the DAB converter where a current overshoot over 8% occurs at worst. The positive current bias can make the transient current I_3 close to zero or even reversely polarized at worst. Both cases can introduce hard switching at I_3 on the secondary bridge due to the existence of dead-time.

The current flowing loops before and after I_3 in Fig. 8 where I_3 is close to zero are illustrated in Fig. 9. When S_{21} and S_{24} are on and S_{22} and S_{23} are off in front of I_3, i_2 flows through the conducting channels of S_{21} and S_{24} as shown in Fig. 9(a). Then, S_{21} and S_{24} switch off, and the secondary bridge enters the sub-cycle of dead-time. During dead-time, i_2 is composed of two parts, the charging current of the parasitic body capacitors of S_{21} and S_{24} and the discharging current of the parasitic body capacitors of S_{22} and S_{23} as shown in Fig. 9(b). Since the absolute value of I_3 is close to zero, both the charging and discharging currents are very weak. Therefore, the charging and discharging processes cannot successfully complete at the end of dead-time. Under this scenario, S_{22} and S_{23} switch on when their parasitic body capacitors are not completely discharged, so zero-voltage-

switching (ZVS) cannot be achieved, and S_{22} and S_{23} switch on with hard switching. Meanwhile, the charging and discharging processes proceed through the conducting channels of S_{22} and S_{23} as shown in Fig. 9(c). When the phase-shift ratio is reduced from 0.5 to 0.04 with T_h/τ=0.7, ΔI_3^* will be over 100% at worst, which means that I_3 will be reversely polarized from negative to positive. In this case, hard switching occurring at I_3 on the secondary bridge is more apparent to observe.

Similarly, the positive current bias during the power decreasing transient from full load to light load can slow down the charging/discharging processes at I_4 and result in hard switching of S_{11} and S_{14} on the primary bridge. In addition, the narrowed soft switching range may have an influence on the subsequent switching actions. In this case, more complicated transient behaviors will happen and cause unexpected problems [28]. It is noteworthy that the turns ratio of the high-frequency transformer can exert an influence on the charging/discharging processes at I_3 and I_4, which will be shown in the experimental results in subsection D of section IV. The hard switching issue may lead to bad EMI and even device failure, therefore reducing the reliability of the DAB converter.

III. PROPOSED PHASE-SHIFT SCHEME CONSIDERING THE RESISTIVE IMPACT

To effectively eliminate the dc current bias for optimal transient response, a modified phase-shift scheme is proposed with T_P and T_S expressions considering the resistive impact. The new solutions are expressed as

$$\begin{cases} T_P = T_h - \tau \ln \dfrac{Me^{-(1-D_2)\frac{T_h}{\tau}}+1}{Me^{-(1-D_1)\frac{T_h}{\tau}}+1} \\ T_S = T_h(1+D_2-D_1) - \tau \ln \dfrac{Me^{-(1-D_2)\frac{T_h}{\tau}}+1}{Me^{-(1-D_1)\frac{T_h}{\tau}}+1} \end{cases} \tag{6}$$

In (6), the time-constant related parameter τ defined in (2) is included to optimize the pulsewidths in Fig. 4 for better transient response. When $R_{eq} = 0$, τ is infinity, and (6) will be simplified into the same form as (1), which shows consistency with the solutions neglecting the resistive impact. In voltage matching mode with $M = 1$, the optimal solutions in (6) become

$$\begin{cases} T_P = T_h - \tau \ln \dfrac{e^{-(1-D_2)\frac{T_h}{\tau}}+1}{e^{-(1-D_1)\frac{T_h}{\tau}}+1} \\ T_S = T_h(1+D_2-D_1) - \tau \ln \dfrac{e^{-(1-D_2)\frac{T_h}{\tau}}+1}{e^{-(1-D_1)\frac{T_h}{\tau}}+1} \end{cases} \tag{7}$$

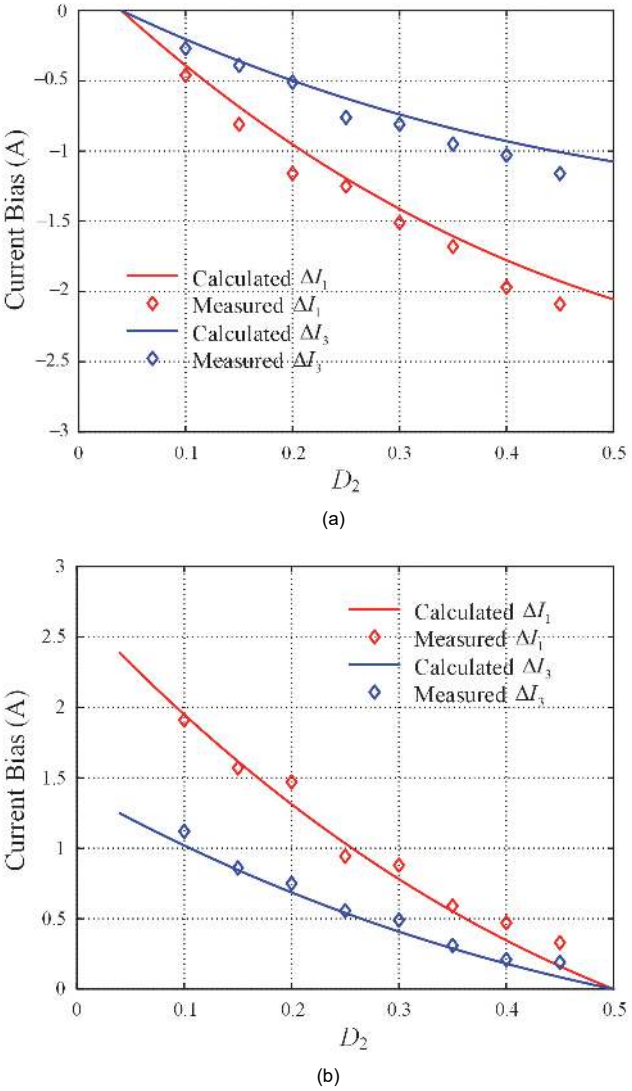

FIGURE 10. Calculated and measured transient dc current bias of I_1 and I_3. (a) Power increasing from D_1=0.04. (b) Power decreasing from D_1=0.5.

For $M = 1$ in voltage matching mode, the conventional solutions neglecting the resistive impact in (1) can be expressed as

$$\begin{cases} T_P = T_h - \dfrac{1}{2}(D_2 - D_1)T_h \\ T_S = T_h + \dfrac{1}{2}(D_2 - D_1)T_h \end{cases} \tag{8}$$

It can be found that the expressions of T_P and T_S in (8) are the limits of those in (7) for $R_{eq} = 0$, which indicates the inherent relation between (7) and (8).

This article has been accepted for publication in a future issue of this journal, but has not been fully edited. Content may change prior to final publication. Citation information: DOI 10.1109/ACCESS.2021.3088839, IEEE Access

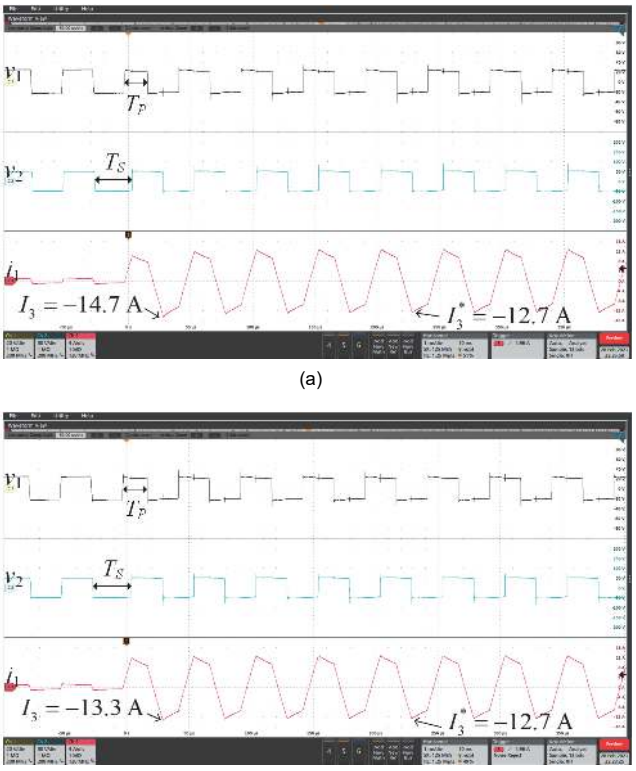

FIGURE 11. Waveforms of v_1 (20 V/div), v_2 (50 V/div), and i_1 (4 A/div) with D_1=0.04 and D_2=0.5. (a) Implemented with the conventional phase-shift scheme neglecting the resistive impact in (8). (b) Implemented with the modified phase-shift scheme considering the resistive impact in (7).

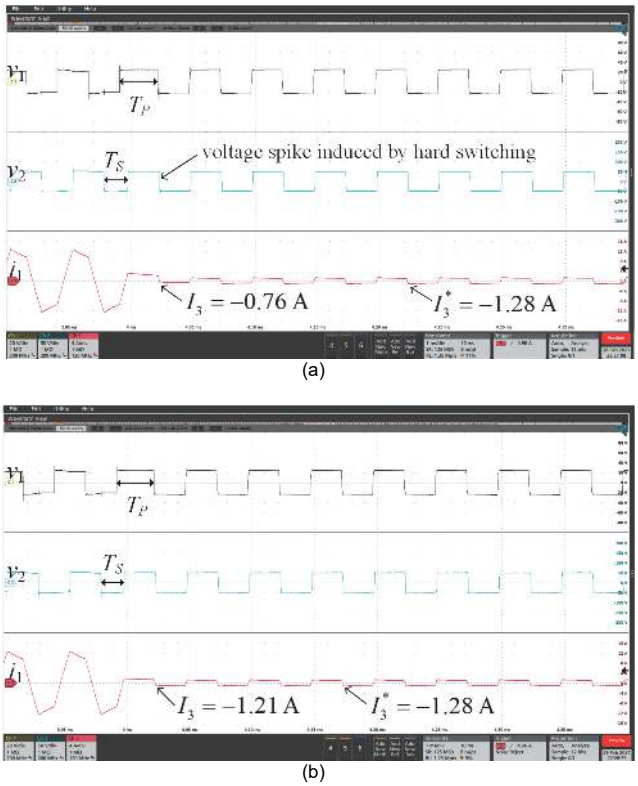

FIGURE 12. Waveforms of v_1 (20 V/div), v_2 (50 V/div), and i_1 (4 A/div) with D_1=0.5 and D_2=0.04. (a) Implemented with the conventional phase-shift scheme neglecting the resistive impact in (8). (b) Implemented with the modified phase-shift scheme considering the resistive impact in (7).

From the discussions in subsection B and subsection C of section II, the resistive impact on the dynamic behaviors is related with T_h/τ. For $T_h/\tau > 3$, the current bias due to the resistive impact is negligible in both power increasing and power decreasing cases, so the simpler solutions in (8) are effective enough for optimal dynamic response. For $0.3<T_h/\tau<1.5$, the resistive impact becomes stronger, and the modified solutions in (7) must be applied for optimal transient performance. In practical applications, τ is usually determined and restricted by the specifications of the converter and considered unchanged, so one of the most feasible ways to mitigate the transient dc bias with the conventional phase-shift solutions in (8) is to reduce the switching frequency to make T_h/τ greater and move far away from the weighting range from 0.3 to 1.5. However, reducing switching frequency may reduce the power density and system efficiency of the converter as well. To avoid the current overshoot and hard switching issues due to transient dc bias and maintain high switching frequency, the proposed phase-shift scheme in (7) will be a good choice if the practical T_h/τ is unavoidably within the weighting range from 0.3 to 1.5. This range is surely subjective, which can be flexibly determined depending on specific applications and designs.

IV. EXPERIMENTAL VERIFICATION

A. EXPERIMENTAL SETUP

In order to verify the above analysis and the proposed phase-shift scheme, a 150 W DAB prototype is constructed. Both the primary and secondary bridges are composed of Infineon IPW60R070CFD7 MOSFETs. The turns ratio of the high-frequency transformer is 21:42, so N=2. A 25 μH auxiliary inductor is installed on the primary side of the transformer. The dc terminals of V_1 and V_2 are connected to two channels of Chroma 17020 Regenerative Battery Pack Test System, which act as two dc buses with constant voltage levels of V_1=25 V and V_2=50 V. The switching frequency is set to 20 kHz, and the dead-time is set to 0.8 μs. The phase-shift algorithms are implemented by PLECS RT Box which provides appropriate gating signals to the MOSFETs. The equivalent-series-resistance of the auxiliary inductor is about 0.18 Ω, the total equivalent resistance of the transformer windings reflected on the primary side is about 0.35 Ω, and the on-resistance of each MOSFET is 0.07 Ω. Therefore, the total equivalent resistance R_{eq} in Fig. 3(b) is about 0.7 Ω. Similarly, the equivalent inductance L_{eq} in Fig. 3(b) is about 27 μH, where the inductance of the auxiliary inductor is 25 μH, and the total equivalent leakage inductance of the transformer reflected on the primary side is about 2 μH. Only the voltage matching mode with $M = 1$ is studied in the following experiments.

B. CURRENT DEVIATION WITH THE CONVENTIONAL PHASE-SHIFT SCHEME NEGLECTING THE RESISTIVE IMPACT

The conventional phase-shift scheme in (8), which neglects the resistive impact, is implemented in the DAB prototype to study the transient current deviation under power changes. The theoretical dc biases of I_1 and I_3 can be calculated and plotted into smooth curves with (4), where the key parameter T_h/τ=0.65. When the power is increased with D_1=0.04 and different values of D_2, the corresponding current deviations, ΔI_1 and ΔI_3, can be measured and recorded in Fig. 10(a) compared with their calculated values. ΔI_1 is the maximum dc bias which does not affect the transient performance directly, while ΔI_3 is the direct factor leading to bad transient response. It is shown that the practical current deviations match the theoretical curves very well with allowable errors. Similarly, when the power is decreased with D_1=0.5 and different values of D_2, the corresponding current deviations, ΔI_1 and ΔI_3, can be measured and recorded in Fig. 10(b) compared with their calculated values. Both the calculated and measured values match each other as well. The errors in Fig. 10(a) and Fig. 10(b) may come from the tolerances of R_{eq} and L_{eq}, voltage ripples in V_1 and V_2, and other possible noisy factors, which are not the dominating factors that seriously affect the transient performance. The experimental results in Fig. 10 verify the correctness of the current deviation analysis in subsection A of section II.

C. INCREASE THE POWER FROM LIGHT LOAD TO FULL LOAD WITH THE MODIFIED PHASE-SHIFT SCHEME (D_1=0.04, D_2=0.5).

The conventional phase-shift scheme in (8) and the proposed phase-shift scheme in (7) are respectively adopted to increase the power from light load (D_1=0.04) to full load (D_2=0.5), and the experimental waveforms are provided in Fig. 11. Since the resistive impact is not considered, there is a negative transient dc bias with the conventional phase-shift scheme in (8) as is shown in Fig. 11(a), where the current deviation of I_3 is about 2 A. This absolute bias is greater than its theoretical value, which is expected to be 1.1 A. That is because the auxiliary inductor L gets slightly saturated due to the current overshoot at I_3. It can be found that there is a down-warping tip at I_3 in Fig. 11(a). The distortion of I_3 is a direct evidence to support the occurrence of magnetic saturation. In contrast, the current deviation is reduced to only 0.6 A with the proposed phase-shift scheme which includes the resistive impact as is shown in Fig. 11(b). The transient performance during power increasing from light load to full load is improved with mitigated current overshoot and fast dynamic response.

D. DECREASE THE POWER FROM FULL LOAD TO LIGHT LOAD WITH THE MODIFIED PHASE-SHIFT SCHEME (D_1=0.5, D_2=0.04).

The conventional phase-shift scheme in (8) and the proposed phase-shift scheme in (7) are respectively adopted to decrease the power from full load (D_1=0.5) to light load (D_2=0.04), and the experimental waveforms are shown in Fig. 12. Since the resistive impact is not considered, there is a positive transient dc bias with the conventional phase-shift scheme in (8) as is shown in Fig. 12(a), where the current deviation of I_3 is about 0.52 A. This absolute bias is smaller than its theoretical value, which is expected to be 1.25 A. That is because the hard switching around I_3 forces the inductor current i_1 to descend for one more period of dead-time. It can be found that the hard switching can induce a voltage spike with the peak-to-peak value of 250 V in v_2. The huge voltage spike may further lead to bad EMI noises and even switching device failure, and therefore reduce the reliability of the converter. In contrast, the current deviation is reduced to only 0.07 A with the proposed phase-shift scheme when the resistive impact is included as is shown in Fig. 12(b). The transient performance during power decreasing from full load to light load is improved as well. The transient dc bias is almost completely removed with the modified solutions in (7). In addition, there is no voltage spike in Fig. 12(b), which indicates that the DAB converter can obtain ZVS during the transient and the soft switching range is maintained even at light load.

It can be observed that there is no hard switching on the primary bridge at I_4 in Fig. 12 (a), although the value of I_4 is as close to zero as I_3. This phenomenon owes to the turns ratio of the high-frequency transformer. The hard switching at I_3 occurs to the secondary bridge, which is the high voltage side, so the actual current flowing through the secondary bridge is further reduced by the transformer's turns ratio. Therefore, the actual charging and discharging currents at I_3 and I_4 are not of the same level. The secondary side current is closer to zero, so it intends to cause hard switching.

V. CONCLUSION

This paper investigates the transient current bias when the conventional phase-shift scheme based on the model without the resistive elements is adopted in a DAB dc/dc converter. It is found that the current bias may cause current overshoot and magnetic saturation for power changes from light load to full load and hard switching for power changes from full load to light load. A modified phase-shift scheme considering the resistive impact is presented which can better eliminate the transient current bias and therefore solve the issues aforementioned. All the conclusions have been verified by experimental results from a 150 W DAB prototype. The proposed phase-shift scheme has been proved to effectively mitigate the current deviation with improved transient response.

APPENDIX

The steady-state peak currents at the turning points in Fig. 2 neglecting the resistive impact can be expressed as [11],

$$\begin{cases} I_0^* = -I_2^* = \dfrac{V_1 T_h (M - 1 - 2MD)}{2L_{eq}} \\ I_1^* = -I_3^* = \dfrac{V_1 T_h (M - 1 + 2D)}{2L_{eq}} \end{cases} \quad \text{(A1)}$$

The steady-state peak currents at the turning points in Fig. 2 considering the resistive impact can be expressed as [24],

$$\begin{cases} I_0^* = -I_2^* = \dfrac{V_1[M - 1 + (1 + M)e^{-\frac{T_h}{\tau}} - 2Me^{-\frac{T_h(1-D)}{\tau}}]}{R_{eq}(1 + e^{-\frac{T_h}{\tau}})} \\ I_1^* = -I_3^* = \dfrac{V_1[M + 1 + (1 - M)e^{-\frac{T_h}{\tau}} - 2e^{-\frac{T_h D}{\tau}}]}{R_{eq}(1 + e^{-\frac{T_h}{\tau}})} \end{cases} \quad \text{(A2)}$$

All the peak current values are just equal to one of the expressions in (A1) or (A2) due to the periodicity of the steady-state waveform of i_1.

REFERENCES

[1] B. Zhao, Q. Song, W. Liu, and Y. Sun, "Overview of dual-active-bridge isolated bidirectional DC–DC converter for high-frequency-link power-conversion system," *IEEE Trans. Power Electron.*, vol. 29, no. 8, pp. 4091–4106, Aug.2014.

[2] F. Krismer and J. W. Kolar, "Efficiency-optimized high-current dual active bridge converter for automotive applications," *IEEE Trans. Ind. Electron.*, vol. 59, no. 7, pp. 2745–2760, Jul. 2012.

[3] Y. Shi, R. Li, Y. Xue, and H. Li, "Optimized operation of current-fed dual active bridge DC–DC converter for PV applications," *IEEE Trans. Ind. Electron.*, vol. 62, no. 11, pp. 6986–6995, Nov. 2015.

[4] J. Hu, P. Joebges, G. C. Pasupuleti, N. R. Averous, and R. W. D. Doncker, "A maximum-output-power-point-tracking-controlled dual-active bridge converter for photovoltaic energy integration into MVDC grids," *IEEE Trans. Energy Convers.*, vol. 34, no. 1, pp. 170–180, Mar. 2019.

[5] F. D. Freijedo, E. Rodriguez-Diaz, and D. Dujic, "Stable and passive high-power dual active bridge converters interfacing MVDC grids," *IEEE Trans. Ind. Electron.*, vol. 65, no. 12, pp. 9561–9570, Dec. 2018.

[6] M. Cupelli *et al.*, "Port controlled hamiltonian modeling and IDA-PBC control of dual active bridge converters for DC microgrids," *IEEE Trans. Ind. Electron.*, vol. 66, no. 11, pp. 9065–9075, Nov. 2019.

[7] J.-Y. Lee, H.-S. Kim, and J.-H. Jung, "Enhanced dual-active-bridge DC–DC converter for balancing bipolar voltage level of DC distribution system," *IEEE Trans. Ind. Electron.*, vol. 67, no. 12, pp. 10399–10409, Dec. 2020.

[8] N. M. L. Tan, T. Abe, and H. Akagi, "Design and performance of a bidirectional isolated DC–DC converter for a battery energy storage system," *IEEE Trans. Power Electron.*, vol. 27, no. 3, pp. 1237–1248, Mar. 2012.

[9] F. Feng, X. Zhang, J. Zhang, and H. B. Gooi, "Stability enhancement via controller optimization and impedance shaping for dual active bridge-based energy storage systems," *IEEE Trans. Ind. Electron.*, to be published, DOI 10.1109/TIE.2020.2992947.

[10] N. Hou and Y. W. Li, "Overview and comparison of modulation and control strategies for a nonresonant single-phase dual-active-bridge DC–DC converter," *IEEE Trans. Power Electron.*, vol. 35, no. 3, pp. 3148–3172, Mar. 2020.

[11] X. Li and Y.-F. Li, "An optimized phase-shift modulation for fast transient response in a dual-active-bridge converter," *IEEE Trans. Power Electron.*, vol. 29, no. 6, pp. 2661–2665, Jun. 2014.

[12] B. Zhao, Q. Song, W. Liu, and Y. Zhao, "Transient DC bias and current impact effects of high-frequency-isolated bidirectional DC–DC converter in practice," *IEEE Trans. Power Electron.*, vol. 31, no. 4, pp. 3203–3216, Apr.2016.

[13] Y. Tang, X. Li, S.-Z. Zhou, C. Sun, and G. Chen, "Comprehensive study of fast load modulation with volt-second balance in a dual-active-bridge converter," *IET Power Electron.*, vol. 12, no. 6, pp. 1357–1367, May 2019.

[14] Z. Ji, Q. Wang, D. Li, and Y. Sun, "Fast DC-bias current control of dual active bridge converters with feedforward compensation," *IEEE Trans. Circuits Syst. II-Express Briefs*, vol. 67, no. 11, pp. 2587–2591, Nov. 2020.

[15] C. Sun and X. Li, "Fast transient modulation for a step load change in a dual-active bridge converter with extended-phase-shift control," *Energies*, vol. 11, no. 6, Jun. 2018, art. no. 1569.

[16] S.-Z. Zhou, C. Sun, S. Hu, G. Chen, and X. Li, "Improved load transient response of a dual-active-bridge converter," in *Proc. IEEE Int. Power Electron. Conf. (IPEC-ECCE Asia)*, Niigata, Japan, May 2018, pp. 370–374.

[17] J. Xu *et al.*, "Fast transient current control for dual-active-bridge DC–DC converters with triple-phase-shift," in *Proc. IEEE Appl. Power Electron. Conf. Expo. (APEC)*, Anaheim, CA, USA, Mar. 2019, pp. 2197–2201.

[18] Q. Bu, H. Wen, J. Wen, Y. Hu, and Y. Du, "Transient DC bias elimination of dual-active-bridge DC–DC converter with improved triple-phase-shift control," *IEEE Trans. Ind. Electron.*, vol. 67, no. 10, pp. 8587–8598, Oct. 2020.

[19] Q. Bu, H. Wen, H. Shi, Y. Hu, and Y. Yang, "Universal transient DC-bias current suppression strategy in dual-active-bridge converters for energy storage systems," *IEEE Trans. Transp. Electrif.*, to be published, DOI 10.1109/TTE.2020.3024200.

[20] K. Takagi and H. Fujita, "Dynamic control and performance of a dual-active-bridge DC–DC converter," *IEEE Trans. Power Electron.*, vol. 33, no. 9, pp. 7858–7866, Sep. 2018.

[21] A. Rodriguez, A. Vazquez, D. G. Lamar, M. M. Hernando, and J. Sebastian, "Different purpose design strategies and Techniques to improve the performance of a dual active bridge with phase-shift control," *IEEE Trans. Power Electron.*, vol. 30, no. 2, pp. 790–804, Feb. 2015.

[22] S. S. Shah and S. Bhattachaarya, "A simple unified model for generic operation of dual active bridge converter," *IEEE Trans. Ind. Electron.*, vol. 66, no. 5, pp. 3486–3495, May 2019.

[23] F. Krismer and J. W. Kolar, "Accurate power loss model derivation of a high-current dual active bridge converter for an automotive application," *IEEE Trans. Ind. Electron.*, vol. 57, no. 3, pp. 881–891, Mar. 2010.

[24] K. Zhang, Z. Shan, and J. Jatskevich, "Large- and small-signal average-value modeling of dual-active-bridge DC–DC converter considering power losses," *IEEE Trans. Power Electron.*, vol. 32, no. 3, pp. 1964–1974, Mar. 2017.

[25] J. A. Mueller and J. W. Kimball, "An improved generalized average model of DC–DC dual active bridge converters," *IEEE Trans. Power Electron.*, vol. 33, no. 11, pp. 9975–9988, Nov. 2018.

[26] S. P. Engel, N. Soltau, H. Stagge, and R. W. D. Doncker, "Improved instantaneous current control for high-power three-phase dual-active bridge DC–DC converters," *IEEE Trans. Power Electron.*, vol. 29, no. 8, pp. 4067–4077, Aug. 2014.

[27] A. Rodriguez, A. Vazquez, D. G. Lamar, M. M. Hernando, and J. Sebastian, "Different purpose design strategies and techniques to improve the performance of a dual active bridge with phase-shift control," *IEEE Trans. Power Electron.*, vol. 30, no. 2, pp. 790–804, Feb. 2015.

[28] B. Zhao, Q. Song, W. Liu, and Y. Sun, "Dead-time effect of the high-frequency isolated bidirectional full-bridge DC–DC converter: Comprehensive theoretical analysis and experimental verification," *IEEE Trans. Power Electron.*, vol. 29, no. 4, pp. 1667–1680, Apr. 2014.

Jian Yin (M'16) received the B.Eng. degree in electrical engineering from the Shandong University, Jinan, China, in 2007, and the Ph.D. degree in electrical and electronic engineering from The University of Hong Kong, Hong Kong, China, in 2015.

He used to be an Electrical Engineer with the Grid Institute of the Shandong Electric Power Engineering Consulting Institute. He is currently an Assistant Professor with the College of Mechatronics and Control Engineering, Shenzhen University, Shenzhen, China. His research interests include bidirectional power converters, wireless power transfer, and advanced motor drives.

Jian Lu received the B.Eng. degree in electrical engineering and automation from the Jingchu University of Technology, Jingmen, China, in 2018. He is currently pursuing the M.Eng. degree with the College of Mechatronics and Control Engineering, Shenzhen University, Shenzhen, China.
His research interests include dual active bridge converters.

Hui Jiang received the B.S. degree from Chongqing University, Chongqing, China, in 1990; and the M.S. and Ph.D. degrees from Hunan University, Hunan, China, in 1999 and 2005, respectively, all in electrical engineering.
She is a Professor with the College of Physics and Optoelectronic Engineering, Shenzhen University, Shenzhen, China. She was a Visiting Scholar at Brunel University, London, UK, from 2005 to 2006. Her research interests include power system economics and power quality analysis and control.

Yitao Liu (S'11–M'15–SM'20) received his B.S. degree in electrical engineering from Wuhan University, Wuhan, China, in 2008; and his M.S. and Ph.D. degrees in electrical and electronic engineering from Nanyang Technological University (NTU), Singapore, in 2009 and 2014, respectively.
He was a Research Fellow at the Rolls Royce-NTU Joint Laboratory from 2014 to 2015. Currently, he is an Assistant Professor with the College of Mechatronics and Control Engineering, Shenzhen University, Shenzhen, China. His research interests include high power density converters, EMI/EMC in power electronics, and wide-band-gap devices.

Jianchun Peng (M'04–SM'17) received the B.S. and M.S. degrees from Chongqing University, Chongqing, China, in 1986 and 1989, respectively, and the Ph.D. degree from Hunan University, Hunan, China, in 1998, all in electrical engineering.
He is a Professor with the College of Mechatronics and Control Engineering, Shenzhen University, Shenzhen, China. He was a Visiting Professor with Arizona State University, Tempe, AZ, from 2002 to 2003; and a Visiting Professor with Brunel University, London, UK, in 2006. His research interests include electricity markets and power system optimal operation and control.